Available online at www.sciencedirect.com
ScienceDirect
Journal of Solid State Chemistry 180 (2007) 62–69
JOURNAL OF SOLID STATE CHEMISTRY
www.elsevier.com/locate/jssc

Syntheses, crystal and electronic structure, and some optical and transport properties of *Ln*CuOTe (*Ln* = La, Ce, Nd)

Min Ling Liu[a], Li Bin Wu[a], Fu Qiang Huang[a,b,*], Li Dong Chen[a], James A. Ibers[b]

[a]*State Key Laboratory of High Performance Ceramics and Superfine Microstructure, Shanghai Institute of Ceramics, Chinese Academy of Sciences, 1295 DingXi Road, 200050 Shanghai, China*

[b]*Department of Chemistry, Northwestern University, 2145 Sheridan Road, Evanston, IL 60208-3113, USA*

Received 18 June 2006; received in revised form 18 September 2006; accepted 18 September 2006
Available online 24 September 2006

Abstract

Three new compounds, LaCuOTe, CeCuOTe, and NdCuOTe, have been synthesized from the respective rare-earth elements, CuO, and a KI flux at 1023 K. The compounds, which have the ZrSiCuAs structure type, are isostructural to LaCuOS, and crystallize in space group $P4/nmm$ of the tetragonal system with two formula units in cells of dimensions at 153 K of $a = 4.1775(5)$ Å, $c = 9.3260(16)$ Å, $V = 162.75(4)$ Å^3 for LaCuOTe; $a = 4.1497(3)$ Å, $c = 9.3090(10)$ Å, $V = 160.30(2)$ Å^3 for CeCuOTe; and $a = 4.1056(9)$ Å, $c = 9.332(4)$ Å, $V = 157.30(8)$ Å^3 for NdCuOTe. The structure of *Ln*CuOTe (*Ln* = La, Ce, Nd) is composed of alternating PbO-like [Ln_2O_2] and anti-PbO-like [Cu_2Te_2] layers stacked perpendicular to [0 0 1]. The experimental optical band gaps of LaCuOTe and NdCuOTe are 2.31 and 2.26 eV, respectively. At 298 K the electrical conductivity of LaCuOTe is 1.65 S/cm and the Hall mobility is $+80.6\,cm^2\,V^{-1}\,s^{-1}$. The positive values of the Seebeck and Hall coefficients indicate *p*-type electrical conduction. First-principles theoretical calculations were performed on LaCuO*Q* (*Q* = S, Se, Te). In LaCuOTe, Cu 3*d* and Te 5*p* orbitals dominate the states near the valence band maximum; the states near the conduction band minimum are composed of Cu 4*s*, Te 5*p*, and La 5*d* orbitals. The larger dispersion of Cu 3*d* orbitals and the presence of Te 5*p* orbitals near the valence band maximum are responsible for the larger hole mobility of LaCuOTe compared to LaCuOS and LaCuOSe.

Keywords: Rare-earth copper oxytelluride; Crystal structure; Optical properties; Transport properties; Electronic structure

1. Introduction

Conductive oxides transparent to visible light are widely used as electrodes for information displays, solar cells, and electrochromic windows [1–3]. Their conductivities in the range of $\sim 10^4\,S\,cm^{-1}$ are similar to those of degenerate semiconductors. However, such high conductivity has so far been achieved only in *n*-type semiconductors, such as Sn-doped In_2O_3 and ZnO-based materials [4,5], whereas the conductivities of transparent *p*-type semiconductors derived from either ZnO (N, As, or P doped) [6–8] or Cu-based compounds ($CuAlO_2$ [9,10], $CuGaO_2$ [11], $CuInO_2$ [12,13], $CuScO_2$ [14], $CuYO_2$ [14], $SrCu_2O_2$ [15], BaCuFS [16], *Ln*CuO*Q* [17–19], where *Ln* = rare-earth metal and *Q* = S or Se) are 10^3–10^4 times lower. The Cu/*Q* materials mostly contain anti-PbO-like [Cu_2Q_2] layers separated by highly ionic atoms or motifs, such as Ba^{2+} or the PbO-like [$Ln_2O_2^{2+}$] layers.

The lanthanum copper oxychalcogenides LaCuO*Q* have been studied extensively owing to their interesting structure and optical and electrical properties [17–26]. The important structural feature of this type of compound is the alternation of stacks of [La_2O_2] and [Cu_2Q_2] layers. Doping by Sr or Ba into the La site of the [La_2O_2] layer can enhance the conductivity of these materials [19,20]. For this reason they have been intensively studied as a promising class of transparent conductive materials. The [Cu_2Q_2] layer, which comprises edge-sharing CuQ_4 tetrahedra, is thought to contain hole transport paths for *p*-type conduction [18,21]. These conduction paths are related to the hybridized Cu 3*d*—*Q np* ($n = 3$ for S, 4 for Se) states at

*Corresponding author. Fax: +8621 52411620.
E-mail address: huangfq@mail.sic.ac.cn (F.Q. Huang).

0022-4596/$ - see front matter © 2006 Elsevier Inc. All rights reserved.
doi:10.1016/j.jssc.2006.09.014

the valence band maximum in the electronic structure. Thus, modification of the anion species can effectively modulate the valence band dispersion near the Fermi level to promote hole mobility and conductivity. LaCuOSe has higher hole mobility and conductivity than does LaCuOS [20]. Because the Cu *3d*—*Q np* hybridization increases in the order of S to Se to Te, we expect LaCuOTe to have higher hole mobility and conductivity than either LaCuOS or LaCuOSe.

The optical properties and the electronic structure of LaCuOTe have been reported [22]. In addition, the lattice constants of some of the other *Ln*CuOTe (*Ln* = rare-earth element) compounds have been determined by powder X-ray diffraction methods [23]. However, their crystal structures as well as their optical and electrical properties have not been studied in depth. In order to understand how the *p*-type transparent conducting properties (both optical and electrical) depend on the chalcogen in *Ln*CuO*Q*, the compounds LaCuOTe, CeCuOTe, and NdCuOTe were synthesized. Their crystal structures were determined from single-crystal X-ray diffraction data. Optical and transport properties were measured and first-principles calculations were performed. These results are reported here.

2. Experimental section

2.1. Syntheses

The following reagents were used as obtained: *Ln* (*Ln* = La, Nd, Ce; Alfa, 99.9%), Ln_2O_3 (*Ln* = La, Nd; Sinoreag., 99.99%), Te (Sinoreag., 99.9%), Cu (Sinoreag., 99.99%), CuO (Sinoreag., 99.9%), and KI (Sinoreag., 98.5%). The Ln_2O_3 oxides were precalcined under an Ar atmosphere at 1273 K for 12 h. *Ln*CuOTe (*Ln* = La, Ce, Nd) were synthesized by the reaction of 1.0 mmol *Ln*, 1.0 mmol CuO, 1.0 mmol Te, and 2.0 mmol KI flux. A reaction mixture was loaded into a fused-silica tube under an Ar atmosphere in a glove box. The tube was sealed under a 10^{-2} Pa pressure, and then placed in a computer-controlled furnace. The sample was heated to 1023 K in 12 h, kept at 1023 K for 72 h, cooled at 3 K/h to 375 K, and then the furnace was turned off. The reaction mixture was washed free of flux with water and then it was dried with acetone. There were two major products: yellow square plates (the desired product) and black powder (unknown phase or phases). The yield of the plates was about 50%. Analysis of the plates with an EDX-equipped Shimadzu EPMA-8705Q instrument indicated the presence of *Ln*, Cu, and Te in the molar ratio of ≈1:1:1; O was observed but could not be quantified. No evidence of K or I was found. The crystals of *Ln*CuOTe are stable in air over months.

A ceramic sample of LaCuOTe was prepared by the reaction of La_2O_3, La, Cu, and Te in the molar ratio 1:1:3:3 without a KI flux. The mixture was first heated in an evacuated fused-silica tube at 723 K for 100 h. This sample was thoroughly ground, pressed into a pellet, and annealed in an evacuated tube at 873 K for 180 h. The sample was then pulverized and ground and characterized as pure LaCuOTe by means of an X-ray diffraction powder pattern obtained on a D/Max 2550 V diffractometer. Finally, it was isostatically pressed into a pellet under 60 MPa and annealed again at 823 K for 12 h. Its purity was again checked by diffraction methods.

A ceramic sample of LaCuOS was prepared in a similar fashion from La_2O_3, La, Cu, and S at 1073 K.

2.2. Crystallography

Single-crystal X-ray diffraction data were obtained for LaCuOTe, CeCuOTe, and NdCuOTe with the use of graphite monochromatized Mo*Kα* radiation (λ = 0.71073 Å) at 153 K on a Bruker Smart-1000 CCD diffractometer [27]. The crystal-to-detector distance was 5.023 cm. Crystal decay was monitored by recollecting 50 initial frames at the end of data collection. Data were collected by a scan of 0.3° in ω in four groups of 606 frames at φ settings of 0°, 90°, 180°, and 270°. The exposure time was 15 s/frame. The collection of the intensity data was carried out with the program SMART [27]. Cell refinement and data reduction were carried out with the use of the program SAINT [27] and face-indexed absorption corrections were performed numerically with the use of the program XPREP [28]. Then the program SADABS [28] was employed to make incident beam and decay corrections.

The structures were solved with the direct-methods program SHELXS and refined with the full-matrix least-squares program SHELXL [28]. Each final refinement included anisotropic displacement parameters. In the *Ln*CuOS series, the lattice volume of CeCuOS does not follow the expected lanthanide contraction but is anomalously small, as deduced from studies of powders [24,25]. This was previously ascribed to nonstoichiometry [24] or to short Ce–S distances [25]. A recent single-crystal study demonstrated that the compound is nonstoichiometric [26]. For this reason a refinement of the structure of CeCuOTe was carried out with the occupancy of the Ce site as an additional variable. The Ce occupancy refined to 0.996(5). Hence, CeCuOTe, as opposed to CeCuOS, is stoichiometric and in the final refinement the occupancy of Ce was set to 1.0. Finally, the program STRUCTURE TIDY [29] was employed to standardize the atomic coordinates. Additional crystallographic details are given in Table 1 and in Supporting information. Table 2 presents selected metrical details.

2.3. Optical absorption and diffuse reflectance measurements

Single-crystal absorption measurements were performed on LaCuOTe and NdCuOTe with the use of an Ocean Optics model S2000 spectrometer over the range of 300–800 nm at 293 K. The spectrometer was coupled

fiber-optically to a Nikon TE300 inverted microscope. White light originated from a TE300 lamp. Each absorption spectrum was collected with light perpendicular to the (001) crystal face.

A UV–Vis–NIR scanning spectrophotometer with a diffuse reflectance accessory (Shimadzu UV-3101) was used to measure the diffuse reflectance spectrum of a powder of LaCuOTe over the wavelength range from 300 to 800 nm at 293 K.

2.4. Electrical conductivity, thermopower, and Hall effect measurements

The electrical conductivity from 150 to 300 K and the Hall effect for LaCuOTe were investigated on an Accent HL5500 Hall System. The conductivities of ceramic bars ($0.4 \times 0.5 \times 1.2$ cm) from 293 to 500 K were also measured by a four-probe technique in a flowing Ar atmosphere. The thermoelectromotive force (E) at 298 K was measured at five different temperature gradients ($0 \leqslant \Delta T \leqslant 10$ K), and the Seebeck coefficient was obtained from the slope of the E versus T plot. Silver paste was used to attach the electrodes, and ohmic contact was confirmed before detailed measurements were made. Excitation currents were kept as low as possible, typically below 1.0 mA, in order to minimize any nonohmic voltage response and thermoelectric effects at the contact–sample interface.

Table 1
Crystal data and structure refinement for *Ln*CuOTe (*Ln* = La, Ce, Nd)[a]

Compound	LaCuOTe	CeCuOTe	NdCuOTe
Formula mass	346.05	347.26	351.38
a(Å)	4.1775(5)	4.1497(3)	4.1056(9)
c(Å)	9.3260(16)	9.3090(10)	9.332(4)
V(Å^3)	162.75(4)	160.30(2)	157.30(8)
ρ_c(g/cm^3)	7.061	7.194	7.419
μ(cm^{-1})	279.8	292.9	318.8
$R(F)$[b]	0.017	0.031	0.020
$R_w(F_o^2)$[c]	0.0439	0.0757	0.0495

[a]For all structures $Z = 2$, space group = P 4/nmm (no. 129), $T = 153$ (2) K, and $\lambda = 0.71073$ Å.
[b]$R(F) = \Sigma||F_o| - |F_c||/\Sigma|F_o|$ for $F_o^2 > 2\sigma(F_o^2)$.
[c]$R_w(F_o^2) = [\Sigma w(F_o^2 - F_c^2)^2/\Sigma wF_o^4]^{1/2}$, $w^{-1} = \sigma^2(F_o^2) + (qF_o^2)^2$ for $F_o^2 > 0$ and $w^{-1} = \sigma^2(F_o^2)$ for $F_o^2 < 0$. $q = 0.025$, 0.055, 0.030 for the La, Ce, Nd compounds, respectively.

2.5. Electronic structure calculations

Electronic structures were calculated by the TB-LMTO program, which is a self-consistent, scalar relativistic linearized muffin-tin orbital program by Andersen and co-workers within the atomic sphere approximation [30–32]. This method splits the crystal space into overlapping atomic spheres. To achieve space filling with the atomic sphere approximation, five empty spheres were introduced for LaCuOQ (Q = S, Se, Te). The positions and radii of the empty spheres were calculated automatically. The radii for the La, Cu, O, S, Se, and Te atoms were also determined automatically to provide overlaps of no more than 16% for any two atom-centered spheres. In the present calculations, the von Barth–Hedin exchange-correlation potential was used within the local density approximation [33]. All k-space integrations were performed with the tetrahedron method with the 108 irreducible k-points that, because of the high symmetry, come from 432 k-points [34,35]. The basis sets consisted of the 4f, 5d, and 6s states for La; the 3d, 4s, and 4p states for Cu; the 2s and 2p states for O; the ns and np states for Q ($n = 3$ for S, 4 for Se, 5 for Te); and the 1s states for empty spheres. The 6p states for La, the nd states for Q, the 3d state for O, and p–d states for empty spheres were downfolded by means of the technique described by Löwdin [36].

3. Results and discussion

3.1. Syntheses

Single crystals of *Ln*CuOTe (*Ln* = La, Ce, Nd) were synthesized in about 50% yield by the reaction of *Ln*, CuO, and Te with a KI flux at 1023 K. These compounds are air-stable. A single-phase ceramic sample of LaCuOTe was prepared from a mixture of La_2O_3, La, Cu, and Te in the molar ratio 1:1:3:3 at 723 K, and annealed at 873 K. The experimental X-ray diffraction pattern of this sample is compared with the theoretical pattern, as simulated from the single-crystal data, in Fig. 1.

Table 2
Selected distances (Å) and bond angles (deg) for *Ln*CuOQ (*Ln* = La, Ce, Nd; Q = S, Se, Te)

Compound	LaCuOTe	CeCuOTe	NdCuOTe	LaCuOS [37]	LaCuOSe [38]
Ln–O × 4	2.3998(3)	2.3831(4)	2.3507(5)	2.367(3)	2.377(1)
Ln–Q × 4	3.4791(5)	3.4515(7)	3.4301(8)	3.253(4)	3.328(3)
Cu–Q × 4	2.6577(4)	2.6602(6)	2.6614(7)	2.437(4)	2.523(3)
Cu···Cu × 4	2.9539(4)	2.9343(2)	2.9031(6)	2.827(1)	2.876(1)
Ln–O–*Ln* × 4	104.03(1)	104.00(2)	103.73(1)	106.6(1)	105.53(5)
Ln–O–*Ln* × 2	121.01(2)	121.07(3)	121.68(3)	115.3(1)	117.67(5)
Q–Cu–Q × 4	112.48(1)	113.06(2)	113.90(2)	109.1(1)	110.52(8)
Q–Cu–Q × 2	103.61(2)	102.52(3)	100.95(3)	110.3(1)	107.40(8)

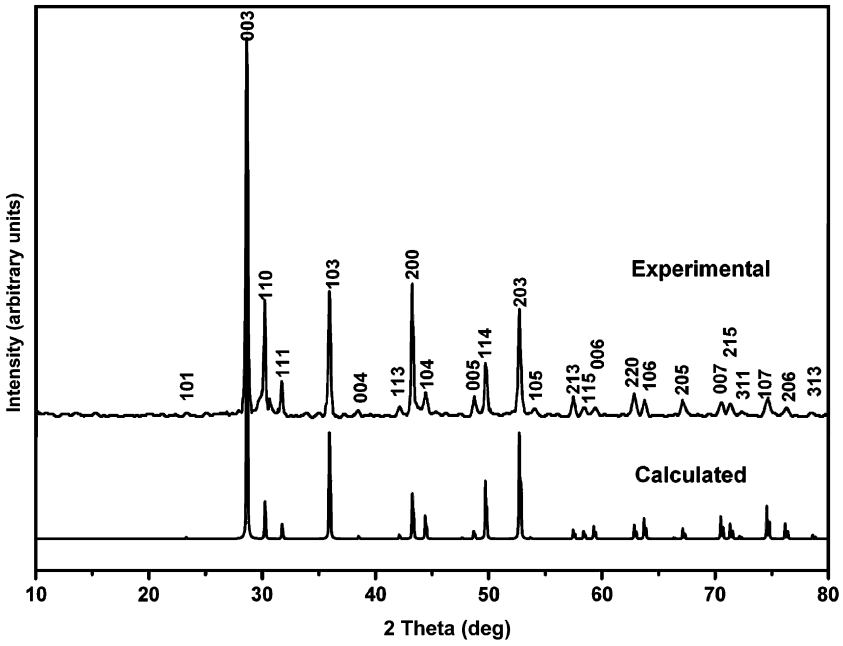

Fig. 1. Experimental and theoretical X-ray diffraction powder patterns of LaCuOTe.

3.2. Crystal structure

The isostructural compounds LaCuOTe, CeCuOTe, and NdCuOTe have the ZrSiCuAs structure type [37], as do the LaCuOQ (Q = S, Se) compounds. These materials crystallize with two formula units in space group $P4/nmm$ of the tetragonal system. The structure (Fig. 2) is composed of alternating PbO-like [Ln_2O_2] and anti-PbO-like [Cu_2Te_2] layers stacked perpendicular to [0 0 1]. These layers are built from edge-sharing OLn_4 and $CuTe_4$ tetrahedra, respectively. In the structure of LnCuOTe, each Ln atom is in the center of a distorted square antiprism with four O atoms in one base and four Te atoms in the other base, as shown in Fig. 3.

Metrical details for these three structures as well as for LaCuOS [38] and LaCuOSe [39] are compared in Table 2. All the Ln–O and Ln–Te distances are typical. For example, compare these to the Nd–O (2.323 Å) and Nd–Te (3.503 Å) bond lengths in Nd_2O_2Te [40]. In LaCuOTe, CeCuOTe, and NdCuOTe the Ln–O, Ln–Te, and Cu⋯Cu distances decrease progressively owing to the lanthanide contraction; as a result the a-axis length also decreases. In the structure of LnCuOTe, each Cu atom (site symmetry $\bar{4}2$m) is coordinated to four Te atoms in a distorted tetrahedron, as shown in Fig. 3. The Cu–Te bond lengths in LnCuOTe are comparable to those of 2.619(7) and 2.695(7) Å in $NaCuZrTe_3$ [41]. The Cu⋯Cu distances are longer in these tellurides than in related compounds; for example the Cu⋯Cu distance is 2.8604(7) Å in $CuAlO_2$ [42], 2.7632(1) Å in $BaCu_2S_2$ [43], 2.827(1) Å in LaCuOS [38], and 2.5865(7)–2.965(1) Å in $La_5Cu_6O_4S_7$ [46]. As shown in Table 2, the Cu⋯Cu distance increases from 2.827(1) Å in LaCuOS [38] to 2.9539(4) Å in LaCuOTe.

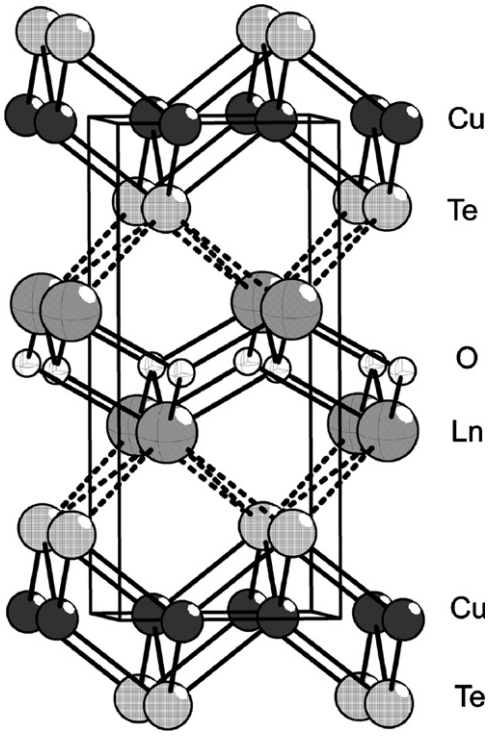

Fig. 2. Crystal structure of LnCuOTe viewed approximately along [1 0 0].

The [La_2O_2] layer also expands in the (001) plane in order to keep the [La_2O_2] and [Cu_2Q_2] layers commensurate. This expansion arises from equal extension of both unshared edges of a hypothetical ideal tetrahedron. The resultant large distortion of the $CuTe_4$ tetrahedron in LaCuOTe may possibly contribute to increased conductivity.

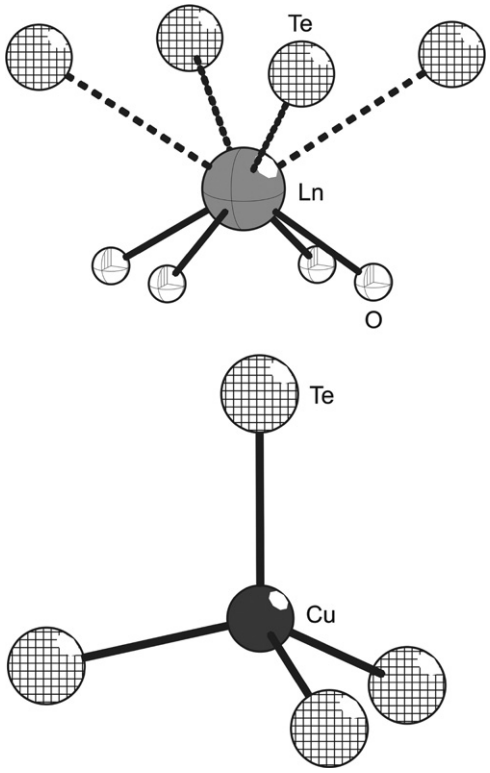

Fig. 3. Coordination environments of *Ln* and Cu in the structure of *Ln*CuOTe (*Ln* = La, Ce, Nd). The site symmetry of *Ln* is 4 mm and that of Cu is $\bar{4}2$ m.

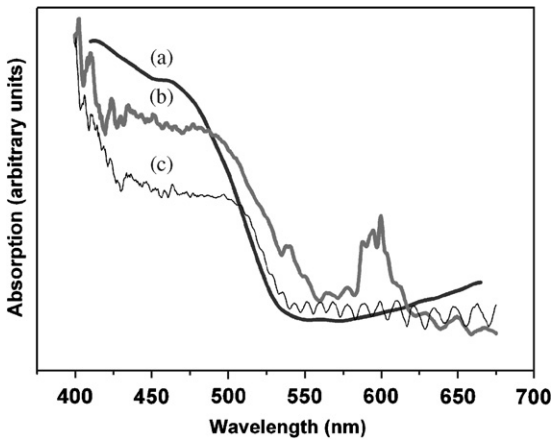

Fig. 4. Optical absorption spectra from (a) ceramic powder of LaCuOTe, (b) single crystal of NdCuOTe, and (c) single crystal of LaCuOTe.

3.3. Optical properties

The absorption spectra obtained from single crystals of LaCuOTe and NdCuOTe with light perpendicular to the (001) face are shown in Fig. 4. The periodic modulation in the spectra at long wavelengths is an interference pattern caused by the finite thickness of the crystals and in NdCuOTe there are also sharp absorption peaks ascribed to Nd^{3+} $4f^4$–$4f^3$ transitions. These artifacts have no influence on the determination of the band gaps, which are 2.31 eV for LaCuOTe and 2.26 eV for NdCuOTe.

The absorption spectrum of a ceramic powdered sample of LaCuOTe at 293 K (Fig. 4) features a sharp drop at about 540 nm (2.29 eV) corresponding to the fundamental absorption edge. The energy gap estimated by extrapolation without taking exciton absorption into account is consistent with the optical band gap measured on the single crystal. Because of the higher energy level of the Te 5*p* level compared to those of S 3*p* and Se 4*p* the band gap in LaCuOTe is narrower than those in LaCuOS (3.1 eV) and LaCuOSe (2.8 eV). The fundamental dependence of the absorption coefficient (α) at different energies is given by the expression $(\alpha h\nu)^n \approx h\nu - E_g$, where E_g is the band gap and $n = \frac{1}{2}$ or 2, respectively, for an indirect allowed or a direct allowed transition [44,45]. The value of n also depends on the shape of the density of states. Fig. 5 shows the plots of $(\alpha h\nu)^2$ and $(\alpha h\nu)^{1/2}$ versus the wavelength λ in the range of 500–540 nm for the LaCuOTe ceramic powder. The band gap is indirect, consistent with an earlier theoretical calculation [22]. By extrapolation of the linear dependence of $(\alpha h\nu)^{1/2}$ versus λ the value of E_g is found to be 542 nm (2.29 eV), consistent with the value derived from the single crystal measurement (Fig. 4).

3.4. Electrical properties

The electrical conductivity (σ) of a bulk ceramic sample of LaCuOTe is shown as a function of temperature (T) in Fig. 6. The material exhibits metallic-like behavior. The decrease of the conductivity with increasing temperature is nearly linear from 150 to 300 K and then parabola-like from 300 to 500 K. The conductivity of LaCuOTe is not very sensitive to temperature, being, for example, 1.95 S/cm at 150 K and 1.35 S/cm at 500 K. LaCuOS and LaCuOSe are both semiconducting. In the LaCuOQ (Q = S, Se, Te) compounds the variation of the conductivity with temperature decreases owing to the increasing hybridization of Cu 3*d* and Q *np* states ($n = 3$ for S, 4 for Se, 5 for Te). Therefore, we may describe LaCuOTe as a degenerate semimetal; a similar degenerate conductivity was found in Mg-doped LaCuOSe [20]. This feature has not been

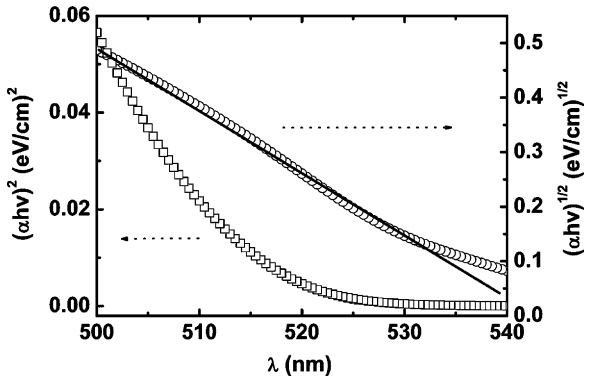

Fig. 5. The dependence of $(\alpha h\nu)^2$ and $(\alpha h\nu)^{1/2}$ versus the wavelength λ in the range of 500–540 nm for the LaCuOTe ceramic powder.

observed among such *p*-type wide band-gap semiconductors as ZnSe:N [47] and GaN:Mg [48].

Table 3 lists some transport properties for $CuAlO_2$ and LaCuO*Q*. The conductivity of the bulk sample of LaCuOS is in the range for the films [17,19]. The conductivity of the bulk sample of LaCuOTe is about 40 times higher than that of bulk LaCuOS, but much lower than that of the LaCuOSe film. The Seebeck and Hall coefficients at 298 K are positive, indicating *p*-type conduction. Note that hole concentration is very sensitive to processing conditions, and a chalcogen-rich atmosphere can increase it [49]. The bulk samples of LaCuO*Q* ($Q = S$, Te) prepared here in evacuated tubes might be *Q*-deficient, resulting in relatively low hole concentrations.

3.5. Electronic structure

The electronic structures of LaCuO*Q* ($Q = S$, Se, Te) were calculated with the use of the TB-LMTO code. The band structure of LaCuOTe (Fig. 7) is similar to those of the other two compounds. Both the highest occupied and the lowest unoccupied states are located at the Γ (0, 0, 0) point. This direct band gap from Γ to Γ is calculated to be 1.96 eV from the local density approximation calculation, smaller than the experimental optical band gap of 2.3 eV. The reason for the difference may be that the discontinuity in the exchange-correlation potential is not taken into account in the present theoretical calculations and thus the energy gap between unoccupied and occupied orbitals is underestimated. Note that in an earlier calculation [22] an indirect band gap was assigned, which is consistent with the experimental results. However, it is very difficult to determine the transition type from theoretical calculations. In the present one, the energy level of the minimum point in the conduction band near the *M* ($\frac{1}{2}$, $\frac{1}{2}$, 0) point is very slightly higher than at the Γ point. However, the lowest unoccupied conduction band near the *M* point is flatter than that near the Γ point. Because a large dispersion in the band structure corresponds to small density states and a small dispersion (flat band) corresponds to large density states, the direct transition Γ to Γ is probably rather weak. The strong optical transition may be the indirect one of flat bands from the valence band near the Γ point to the conduction band near the *M* point.

Fig. 8 shows the total and partial (Cu, *Q*) density of states (DOS) for LaCuO*Q* ($Q = S$, Se, Te). The O states make few contributions around the Fermi level, and the only contributions from the La 5*d* states are near the conduction band minimum. The La 4*f* states in LaCuOTe distribute above 4 eV, and shift to higher energies in the LDA + U calculations [22]. In LaCuOTe, the valence band

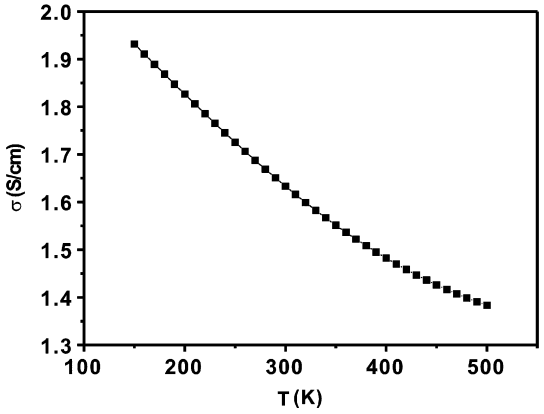

Fig. 6. The electrical conductivity (σ) of LaCuOTe as a function of temperature (*T*).

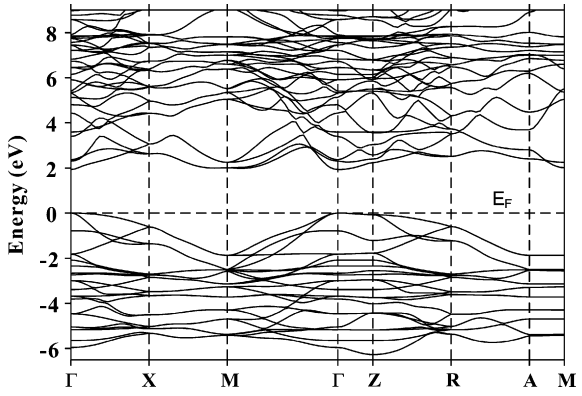

Fig. 7. The band structure of LaCuOTe. The special *k*-points are Γ (0, 0, 0), *X* ($\frac{1}{2}$, 0, 0), *M* ($\frac{1}{2}$, $\frac{1}{2}$, 0), Z (0, 0, $\frac{1}{4}$), *R* (0, $\frac{1}{2}$, $\frac{1}{4}$), and *A* ($\frac{1}{2}$, $\frac{1}{2}$, $\frac{1}{4}$).

Table 3
Electrical properties of $CuAlO_2$ and LaCuO*Q* ($Q = S$, Se, Te)

Sample	Cond. σ (S/cm)	Hall coeff. μ ($cm^2 V^{-1} s^{-1}$)	Holes *n* (cm^{-3})	Seebeck coeff. *S* ($\mu V K^{-1}$)	Band gap E_g (eV)	Ref.
$CuAlO_2$ film	9.5×10^{-2}	10.4	1.3×10^{17}	+183	3.1	9
LaCuOS film[a]	1.2×10^{-2}	~0.5	1.5×10^{17}[b]	+150	3.1	17,20
	6.4×10^{-5}	0.20	2.0×10^{15}	+713	3.1	19
LaCuOS bulk	4.5×10^{-3}	9.39	3.0×10^{15}	+134	3.1	This work
LaCuOSe film	24	8	1.9×10^{19}[b]	~+230	2.8	20
LaCuOTe bulk	1.65	80.6	1.3×10^{17}	+310	2.3	This work

[a]The data were sensitive to the deposition conditions, including radio frequency power, atmosphere, and substrate temperature.
[b]The value was estimated from $n = \sigma/q\mu$.

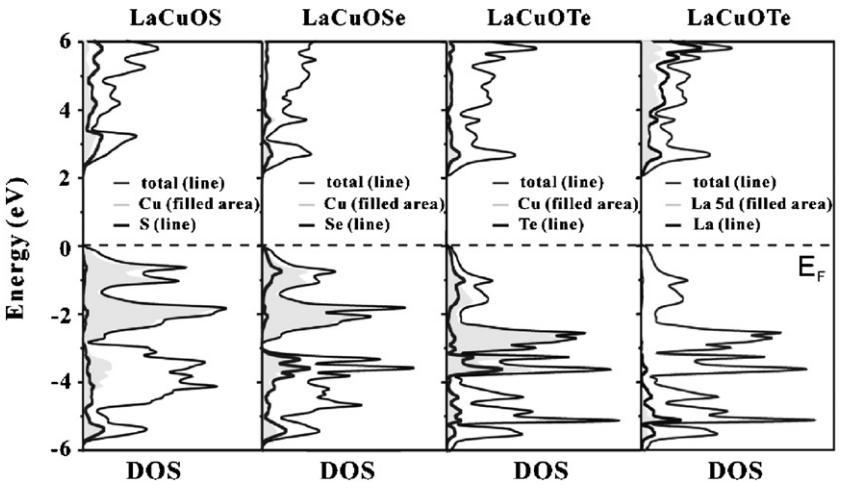

Fig. 8. Total and partial density of states (DOS) of LaCuOQ (Q = S, Se, Te), where the valence band maximum is dominated by Cu 3d and Q np states and the conduction band minimum is composed of the hybridized Cu 4s, Q np, and La 5d states.

maximum is dominated by Cu 3d and Te 5p states, and the conduction band minimum is composed of the hybridized Cu 4s, Te 5p, and La 5d states. Thus, the electronic properties of p-type conduction are mainly determined by the [Cu_2Te_2] layer. As indicated in Fig. 8, the major distribution of the occupied S 3p states is much lower in energy than that of the Te 5p states. Therefore, Cu 3d–S 3p hybridization in LaCuOS is weaker than Cu 3d–Te 5p hybridization in LaCuOTe. The dispersion of Cu 3d states near the valence band maximum for LaCuOQ increases in the order of S to Se to Te. Therefore, compared to LaCuOS and LaCuOSe, the larger dispersion of the Cu 3d states and increased distribution of Te 5p states near the valence band maximum are responsible for the hole mobility in LaCuOTe. Note that p-type doping is easy in tellurides and difficult in the more electronegative oxides and sulfides owing to the incorporation of Te 5p states that lift the valence band maximum above the "p-type pinning energy" $E_F^{(p)}$ [50].

The short Cu⋯Cu distances and the hybridization of Cu 3d and O 2p (S 3p) states in the p-type Cu-based transparent conductors result in their p-type electrical conductivities [50]. The Cu–Te bond length and the distortion of the $CuTe_4$ tetrahedron can influence the Cu 3d–Te 5p hybridization. A longer Cu–Te bond results in weaker binding strength, less electron overlap, and a smaller energy gap between the bonding and antibonding molecular orbitals of the Cu–Te bond. With ideal tetrahedral symmetry (T_d), the Cu 3d states adopt the scheme of three (T_2) over two (E). In LnCuOTe, the $CuTe_4$ tetrahedron has D_{2d} symmetry, and the triply degenerate T_2 states split into B_2 and E and the doubly degenerate E states split into A_1 and B_1, leading to a larger dispersion of Cu 3d states, the hybridization of Cu 3d and Te 5p states in a broader range, and a narrower energy gap. Through the introduction of different Ln, the transport and optical properties may be tuned.

4. Supporting information

The crystallographic files in cif format for LaCuOTe, CeCuOTe, and NdCuOTe have been deposited with FIZ Karlsruhe as CSD numbers 416522, 416521, and 416523, respectively. These data may be obtained free of charge by contacting FIZ Karlsruhe at +49 7247 808 666 (fax) or crysdata@fiz-karlsruhe.de (email).

Acknowledgments

Financial support from the NSF of China (Grant no. 20471068) is acknowledged. This work was supported in part by US Department of Energy BES Grant ER 15522. Use was made of the MRL Central Facilities supported by the US National Science Foundation at the Materials Research Center of Northwestern University under Grant no. DMR00-76097.

References

[1] G. Thomas, Nature 389 (1997) 907–908.
[2] J.F. Wager, Science (Washington, DC, US) 300 (2003) 1245–1246.
[3] H. Ohta, H. Hosono, Mater. Today 7 (6) (2004) 42–51.
[4] K. Nomura, H. Ohta, K. Ueda, T. Kamiya, M. Hirano, H. Hosono, Science (Washington, DC, US) 300 (2003) 1269–1272.
[5] K. Nomura, H. Ohta, A. Takagi, T. Kamiya, M. Hirano, H. Hosono, Nature 432 (2004) 488–492.
[6] M. Sanmyo, Y. Tomita, K. Kobayashi, Chem. Mater. 15 (2003) 819–821.
[7] J.M. Bian, X.M. Li, X.D. Gao, W.D. Yu, L.D. Chen, Appl. Phys. Lett. 84 (2004) 541–543.
[8] J.-R. Duclère, M. Novotny, A. Meaney, R. O'Haire, E. McGlynn, M.O. Henry, J.-P. Mosnier, Supperlattices Microstruct. 38 (2005) 397–405.
[9] H. Kawazoe, M. Yasukawa, H. Hyodo, M. Kurita, H. Yanagi, H. Hosono, Nature 389 (1997) 939–942.
[10] B.J. Ingram, G.B. González, T.O. Mason, D.Y. Shahriari, A. Barnabè, D. Ko, K.R. Poeppelmeier, Chem. Mater. 16 (2004) 5616–5622.

[11] K. Ueda, T. Hase, H. Yanagi, H. Kawazoe, H. Hosono, H. Ohta, M. Orita, M. Hirano, J. Appl. Phys. 89 (2001) 1790–1793.
[12] H. Yanagi, T. Hase, S. Ibuki, K. Ueda, H. Hosono, Appl. Phys. Lett. 78 (2001) 1583–1585.
[13] H. Yanagi, K. Ueda, H. Ohta, M. Orita, M. Hirano, H. Hosono, Solid State Commun. 121 (2001) 15–17.
[14] N. Duan, A.W. Sleight, M.K. Jayaraj, J. Tate, Appl. Phys. Lett. 77 (2000) 1325–1326.
[15] B.J. Ingram, B.J. Harder, N.W. Hrabe, T.O. Mason, K.R. Poeppelmeier, Chem. Mater. 16 (2004) 5623–5629.
[16] H. Yanagi, J. Tate, S. Park, C.-H. Park, D.A. Keszler, Appl. Phys. Lett. 82 (2003) 2814–2816.
[17] K. Ueda, S. Inoue, S. Hirose, H. Kawazoe, H. Hosono, Appl. Phys. Lett. 77 (2000) 2701–2703.
[18] K. Ueda, S. Inoue, H. Hosono, N. Sarukura, M. Hirano, Appl. Phys. Lett. 78 (2001) 2333–2335.
[19] H. Hiramatsu, M. Orita, M. Hirano, K. Ueda, H. Hosono, J. Appl. Phys. 91 (2002) 9177–9181.
[20] H. Hiramatsu, K. Ueda, H. Ohta, M. Hirano, T. Kamiya, H. Hosono, Appl. Phys. Lett. 82 (2003) 1048–1050.
[21] K. Ueda, S. Hirose, H. Kawazoe, H. Hosono, Chem. Mater. 13 (2001) 1880–1883.
[22] K. Ueda, H. Hisono, N. Hamada, J. Phys.: Condens. Matter 16 (2004) 5179–5186.
[23] B.A. Popovkin, A.M. Kusainova, V.A. Dolgikh, L.G. Aksel'rud, Russ. J. Inorg. Chem. 43 (1998) 1471–1475.
[24] D.O. Charkin, A.V. Akopyan, V.A. Dolgikh, Russ. J. Inorg. Chem. 44 (1999) 833–837.
[25] K. Ueda, K. Takafuji, H. Hosono, J. Solid State Chem. 170 (2003) 182–187.
[26] G.H. Chan, B. Deng, M. Bertoni, J.R. Ireland, M.C. Hersham, T.O. Mason, R.P. Van Duyne, J.A. Ibers, Inorg. Chem. 45 (2006) 8264–8272.
[27] Bruker, SMART Version 5.054 Data Collection and SAINT-Plus Version 6.45a Data Processing Software for the SMART System. Bruker Analytical X-ray Instruments, Inc., Madison, WI, USA. 2003.
[28] G.M. Sheldrick, SHELXTL Version 6.14, Bruker Analytical X-ray Instruments, Inc., Madison, WI, USA. 2003.
[29] L.M. Gelato, E. Parthé, J. Appl. Crystallogr. 20 (1987) 139–143.
[30] O.K. Andersen, Phys. Rev. B 12 (1975) 3060–3083.
[31] O.K. Andersen, O. Jepsen, Phys. Rev. Lett. 53 (1984) 2571–2574.
[32] O. Jepsen, O.K. Andersen, Z. Phys. B: Condens. Matter 97 (1995) 35–47.
[33] L. Hedin, B.I. Lundqvist, J. Phys. Chem. Solids 4 (1971) 2064–2083.
[34] W.R.L. Lambrecht, O.K. Andersen, Phys. Rev. B 34 (1986) 2439–2449.
[35] O. Jepsen, O.K. Andersen, Solid State Commun. 9 (1971) 1763–1767.
[36] P.-O. Löwdin, J. Chem. Phys. 19 (1951) 1396–1401.
[37] V. Johnson, W. Jeitschko, J. Solid State Chem. 11 (1974) 161–166.
[38] M. Palazzi, C. R. Acad. Sci. Sér. 2 292 (1981) 789–791.
[39] K. Ueda, H. Hosono, Thin Solid Films 411 (2002) 115–118.
[40] F.A. Weber, T. Schleid, Z. Anorg. Allg. Chem. 625 (1999) 1833–1838.
[41] M.F. Mansuetto, P.M. Keane, J.A. Ibers, J. Solid State Chem. 105 (1993) 580–587.
[42] T. Ishiguro, A. Kitazawa, N. Mizutani, M. Kato, J. Solid State Chem. 40 (1981) 170–174.
[43] J. Huster, W. Bronger, Z. Anorg. Allg. Chem. 625 (1999) 2033–2040.
[44] T.-H. Bang, S.-H. Choe, B.-N. Park, M.-S. Jin, W.-T. Kim, Semicond. Sci. Technol. 11 (1996) 1159–1163.
[45] J.J. Pankove, Optical Processes in Semiconductors, Prentice-Hall, Inc., Englewood Cliffs, NJ, 1971.
[46] F.Q. Huang, P. Brazis, C.R. Kannewurf, J.A. Ibers, J. Solid State Chem. 155 (2000) 366–371.
[47] J. Qui, J.M. DePuydt, H. Cheng, M.A. Haase, Appl. Phys. Lett. 59 (1991) 2992–2994.
[48] S.C. Jain, M. Willander, J. Narayan, R. Van Overstraeten, J. Appl. Phys. 87 (2002) 965–1006.
[49] H. Hiramatsu, K. Ueda, H. Ohta, M. Orita, M. Hirano, H. Hosono, Thin Solid Films 411 (2002) 125–128.
[50] A. Zunger, Appl. Phys. Lett. 83 (2003) 57–59.